Brazilian Journal of Geophysics, **42** (2024), 1, 1–15
Brazilian Geophysical Society
ISSN 2764-8044
DOI 10.22564/brjg.v41i1.2295

3D REFRACTION TRAVELTIME ACCURACY STUDY IN HIGH CONTRASTED MEDIA

Paulo H. B. Alves [1*], Luiz A. Santos [1,2], Felipe V. Capuzzo [1], and Marco Cetale [1]

[1]Universidade Federal Fluminense - UFF, PPGDOT, GISIS, Niterói, RJ, Brazil
[2]Petrobras, Rio de Janeiro, RJ, Brazil

*Corresponding author: pbastos@id.uff.br

ABSTRACT. Among all the existing methods to solve the eikonal equation, three methods are chosen to verify accuracy, symmetry, reciprocity and error propagation along large offsets of refracted waves in seismic near surface exploration context. Performance is extremely highlighted nowadays and accuracy is being neglected, then an eikonal solver poorly explored in geoscience is used. A classical solver, the Fast Iterative and the modified Fast Sweeping Method are applied in three modeling schemes: a simple two layers model, a large four layers and a complex benchmark model. The three methods compute the first arrival of refracted waves in high contrast media and the results are compared to the analytical solution. A circular geometry is considered in all experiments to explore the method applicability using full azimuth angles. On the first scheme, the errors in traveltime are computed among the three methods using different model sample spacing and we discuss accuracy, symmetry and reciprocity of first arrivals. On the second scheme, three circular receivers are placed in different offsets to check errors along refracted wave propagation. Finally, the third scheme, four shots are strategically positioned over the SEG/EAGE Overthrust model in order to compare the full acoustic wavefield with the eikonal solvers and then check the similarities. Although the focus is on methods accuracy, the algorithm run time is also considered and the comparison shows that the modified Fast Sweeping Method is the most accurate. The most computational efficient eikonal solver is the Fast Iterative Method, but its geoscience applicability needs to be cautious, because of its inaccurate results.

Keywords: eikonal solvers; refracted waves; numerical - analytical comparison; accurate first arrivals.

INTRODUCTION

There is a number of refracted wave applications in exploration seismology such as migration (Shen and Zhang, 2020), illumination study to reservoir monitoring (Lopez et al., 2020) and, most often, in seismic tomography. Comparing eikonal and ray-tracing based tomography in a cross well survey, Balkaya et al. (2010) conclude that the eikonal kernel inversion obtains better reconstruction of sharp structures. Besides, Farra (1993) shows that a smoothed model is the solution for the instability of ray-tracing equations and, due to this, the eikonal equation is highly recommended to compute traveltimes in strongly contrasted media. An iterative solution for the eikonal equation is developed by Vidale (1988); then, novel solvers are proposed (Van Trier and Symes, 1991; Podvin and Lecomte, 1991; Qin et al., 1992; Hole and Zelt, 1995). Currently efforts are being directed to the wavefront expansion solvers, such as Group Marching Method (Qin et al., 1992), Fast Marching Method Sethian (1999) and Fast Iterative Method Jeong and Whitaker (2008). The Fast Sweeping Method appears as a great solver as it is demonstrated in Capozzoli et al. (2013), whose study compares the time execution of Fast Marching, Fast Iterative and Fast Sweeping methods in homogeneous media and in a maze model. The Fast Iterative Method performs better than the others, but nothing is shown about accuracy. The strategy of using refracted waves with large offset shot circles in Ocean Bottom Node geometry is being applied to monitoring and characterizing reservoirs in the pre-salt Brazilian Santos basin (Lopez et al., 2020; Costa et al., 2020; Da Silva et al., 2022). Following

this acquisition geometry, but using refracted traveltimes, the objective of this paper is to verify, through a comparison with an analytical solution for refracted waves, eikonal solver accuracy and reciprocity of three methods: the classic (Podvin and Lecomte, 1991), the Fast Iterative (Jeong and Whitaker, 2008) and a variation of the Fast Sweeping Method (Noble et al., 2014). Reciprocity is taken into account because in Tryggvason and Bergman (2006) it is shown a discrepancy error in the classical methodology and then a solution is proposed. The application of an accurate method in high contrasted media may bring more information for inversion and migration.

Firstly, in the following section, we describe equations, methodology and detail the modeling schemes to compare analytical and numerical solutions of traveltimes. The first approach is the simplest to verify symmetry, reciprocity and precision of first arrival traveltimes. The second approach is used to verify traveltime errors along offsets, so interfaces are strategically positioned to pick the time at each circle geometry. The third approach, the last scheme, illustrates the wave propagation comparison with first arrivals in the SEG/EAGE Overthrust model. Thus, the acoustic wave equation is solved using finite difference stencils and the first arrival amplitude is compared with the first arrival traveltimes. The Results and Discussion sections show all figures to verify the simulations and, although the focus of this work is the accuracy of the methods, we discuss the computational time in each experiment. Finally, the Conclusion section points out the considerations of the analysis of accuracy and performance for each experiment and method.

METHODOLOGY

The target phenomenon to be studied in this research is the head waves, the one that are refracted whenever the incident angle is higher than the critical angle (Sheriff and Geldart, 1995). We can generate head waves using the high frequency approximation of the wave equation for isotropic and acoustic media, the Eikonal equation:

$$\left(\frac{\partial T}{\partial x}\right)^2 + \left(\frac{\partial T}{\partial y}\right)^2 + \left(\frac{\partial T}{\partial y}\right)^2 = \frac{1}{v^2(z,x,y)}, \quad (1)$$

where $T = T(z,x,y)$ in 3D case is the first arrival volume and $v = v(z,x,y)$ velocity model, $v(z,x,y)$. Because we are considering the isotropic formulation, the ray is orthogonal to the wavefronts and may be calculated as the gradient of the traveltime volume (Robinson and Clark, 2017). The first arrivals correspond to the exact solution of an elastodynamic equation and build a complete wavefield based on a known velocity model (Cervenỳ, 2001). Therefore, the eikonal solvers try to apply numerical methods to solve the spatial partial derivatives over traveltimes present in Equation (1). The most famous methodology is the Finite Difference Method that approximates the derivatives using the Taylor series function over model grid points depending on the approximation order. Different from the classical wave equation solution, the operators are built considering the near neighbour grid points and to improve accuracy more neighboring points are used (Ahmed et al., 2011; Cai et al., 2023).

Analytical solution

A general formulation is used to calculate analytical traveltimes for n horizontal layers (Kearey et al., 2002). It is needed the distance between source and receiver (offset), the 1D velocity model and the thickness of all layers. The main equation is given below:

$$t_n = \frac{x}{v_n} + \sum_{i=1}^{n-1} \frac{2z_i \cos(\theta_{in})}{v_i}; \quad \theta_{in} = \sin(v_i/v_n), \quad (2)$$

where t_n is the traveltime for each layer n; x is the offset; z_i and v_i are the thickness and the velocity of each layer i, respectively; and θ_{in} is the incident critical angle for each layer. The generalization scheme and a simplification for three layers is shown in Figure 1. This scheme is used to compute analytical traveltimes to compare with numerical solutions described in the next sections.

Classical method

The method chosen to be the main reference for this study is the Podvin and Lecomte (1991) formulation. This methodology is broadly used to compute first arrival traveltimes in geoscience problems. Linde et al. (2008) perform a 2D joint inversion using structural constraints, Yordkayhun et al. (2009) map through a 3D traveltime tomography to monitoring CO_2 migration in a saline aquifer, De Matteis et al. (2010) explore a statistical analysis to estimate model uncertainty and resolution in 3D first arrival tomography and Bulhões et al. (2021) study the regularization effects using first arrival tomography in shallow models. All those works are related to inversion problems but using Podvin and Lecomte (1991) formulation as the modeling kernel. Despite the high applicability, some limitations can be found, such as in Tryggvason and Bergman (2006), where it can be found discrepancies in the calculation of times using reciprocity, and in Koketsu (2000), where instability of times using models with irregular interfaces can be found.

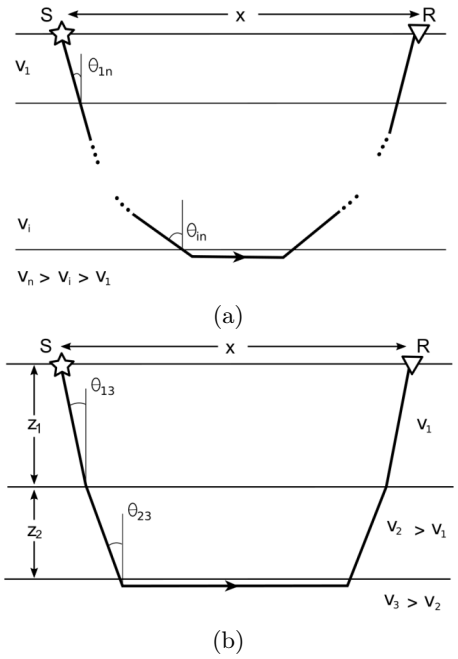

Figure 1: (a) Analytical solution for n planar layers; b) Simplification for three layers adapted from Kearey et al. (2002). S is used to reference the source position and R is used to show the receiver position, both on the same elevation. x is the offset and z the thickness of each layer. θ is the incidence critical angle related with the interface velocity contrast. The velocity always increases with depth and there is no lateral velocity variation inside each layer.

Based on the finite difference approximation, the classical method uses a systematic application of Huygens principle, where each wavefront expansion can behave as a source that expands another wavefront. Because of that, causality is respected in propagation. This numerical method discretizes Equation (1) and builds finite difference operators that can use the neighboring points to derive 1D, 2D and 3D operators. The model is constructed as a regular grid volume, and some of conditional operators are applied to check illumination at each grid point computed. In the 3D case computation, up to 170 stencils are applicable: six 1D transmitted arrivals, twenty-four 2D transmitted arrivals (conditional), twelve 2D diffracted arrivals, ninety-six 3D transmitted plane wavefront (conditional) and thirty-two 3D diffracted arrivals (Podvin and Lecomte, 1991). The number of iterations is computed based on the distance from the source position to the end of the model in samples. An auxiliary volume is stored at each iteration to save grid points that were computed using the expanding cube methodology. All finite difference operators are computed in order to find the smaller traveltime. It is necessary to compute the analytical traveltime from source to the nearest grid point in meters to compute the first arrivals outside a grid point. Trilinear interpolation is applied to register time at the receiver outside the grid point. The process to compute traveltimes at each grid point is independent, so parallel computing is possible. Thus, the algorithm is parallelized using OpenACC compilation directives in the C++ programming language (Farber, 2016).

Fast Iterative Method

The Fast Iterative Method (Jeong and Whitaker, 2008) improved the performance of eikonal equation solvers, and was inspired by the Fast Marching method (Sethian, 1999) and other wavefront expansion methods. This methodology is highly used in GPU parallelization approach, and many benchmark execution time tests are available in different parallel distributions. Dang and Emad (2014) investigate two parallel level approaches working with asynchronous communication. Hong and Jeong (2016) solve the method using multi-GPU system, and Huang (2021) manages the algorithm to improve the performance of the method. All those works only prioritize performance. The Fast Iterative Method tries to formulate a cheapest alternative algorithm that beats the famous and broadly applied geoscience Fast Marching Method because of its simplicity and high performance. The Sethian (1999) method is broadly developed such as Rawlinson and Sambridge (2004, 2005) and shows the availability to handle wave propagation in heterogeneous media. Herrmann (2003); Yang and Stern (2017) use domain decomposition to make the Fast Marching Method parallelizable. Although Cai et al. (2023) has tested the accuracy and proposed an improved formulation, the methodology of Jeong and Whitaker (2008) has not been compared with other formulations in terms of accuracy.

The Fast Iterative Method was chosen because Capozzoli et al. (2013) show its higher computational performance over the Fast Marching Method for a homogeneous medium. Despite thee fact that we record run time experiments, we focus our study on the accuracy of the calculated traveltime. The Fast Iterative Method kernel equation is empirically formulated based on well-known eikonal equation solvers (Jeong and Whitaker, 2008). The algorithm proposes a list scheme: the updated points, the wavefront points (active list) and the external points. The iterative process solves the equation using only the wavefront points, avoiding computational effort in all grid points. The active list, at the beginning of the simulation, contemplates only the nearest source neighboring points. After the update, the active list is emptied, new points are added to the active list, and a new iteration starts in a process such as wavefront expansion. In this study, the original scheme of lists is not employed. To propagate traveltimes using the Fast Iterative Method, only the kernel equation and the expanding cube methodology are applied. In our implementation, to initialize a source outside the grid points we compute the analytical time from the source position to the nearest grid point in meters, and we

register the traveltime outside the grid points, performing a trilinear interpolation.

Accurate Fast Sweeping Method

The Fast Sweeping Method, originally created by Zhao (2005), is an iterative formulation to improve finite difference operators to compute eikonal solvers. The method sweeps the entire 3D domain in different directions reducing computational cost in serial computing when compared to Podvin and Lecomte (1991) formulation that solve the operators in cascade. Bak et al. (2010) show how the Fast Sweeping Method can be better than the Fast Marching Method in strong velocity contrasts using some sweeping domain variations. Zhao (2007) illustrates the first attempt of the parallelized Fast Sweeping Method and Detrixhe et al. (2013) show that the Zhao (2007) method cannot be parallelized on large scale, and proposed a better solution that solves the problem efficiently. The Fast Sweeping Method is broadly applied using anisotropic media (Luo and Qian, 2012; Waheed et al., 2015; Waheed and Alkhalifah, 2017; Huang and Luo, 2020) with great feasibility for realistic applications. Focusing on accuracy, Noble et al. (2014) created a hybrid Accurate Fast Sweeping Method for the eikonal equation on isotropic media using Spherical and Cartesian finite difference operators. The main innovation of this method is the expanded 8-point finite difference operator originally from Vidale (1988), that shows in truncated form. The Spherical operators are applied near the source to fit the wavefront spherical behavior and the Cartesian operators are applied over other grid points far from the source. With the expansion of the 8-points operator Vidale (1988), the precision increases and some operators can be discarded to improve the execution time (Noble et al., 2014). In this paper, just the Cartesian operators are used with no parallelization following the 3D code in the github repository of Noble et al. (2014). An important aspect to emphasize about the Noble et al. (2014) formulation is that the points around the source need to be initialized with analytical traveltimes. There is a step before the global sweep that sweeps the domain using the source position as the reference to start sweeping up to edges of domain called initial sweep. This step makes the Fast Sweeping Method converge into only one iteration for most of the average subsurface models. As in other previous methods presented in this paper, the receivers outside the grid register traveltimes using a trilinear interpolation of neighboring points.

Modeling schemes

The first scheme of this study is related with symmetry and reciprocity accuracy analysis. Thus, a simple model is applied and the sample spacing is changed to verify the effects of the grid size. The common used discretization parameters applied are 100, 50 and 25 meters (m). The model dimensions, considering the (z, x, y) format, are (1.1, 22, 22) kilometers (km). The total samples of models are (12, 221, 221), (23, 441, 441) and (45, 881, 881) homogeneous grid for a spacing of 100, 50, 25 m, respectively. Figure 2 shows the acquisition geometry, a velocity log and vertical model slices to illustrate all approach 1 configuration. The acquisition geometry has 5 shots positioning at 1 - (0, 1, 1); 2 - (0, 1, 21); 3 - (0, 21, 1); 4 - (0, 21, 21); and 5 - (0, 11, 11) km. the shots are strategically positioned to verify the symmetry between shots 1 and 3, and 2 and 4. Shot 5 is used to verify the reciprocity propagation, when the receiver and shot positions are interchanged. The receiver configuration is circular, and the center is located at (0, 11, 11) km with a radius of 10 km and a circular distance of 12.5 m of between them.

The second scheme analyzes errors during the wavefront propagation between layers. Figure 3 shows the entire configuration of how the acquisition geometry was chosen, the velocity model interfaces and the raypath distribution at each layer. The model dimensions are (4.5, 27, 27) km, in the (z, x, y) format; the sample spacing is 25 m; and the model has (181, 1081, 1081) samples. Just one source at the center of the model is applied to check all azimutal signature of traveltimes. The layer interfaces are located at 1, 2.4 and 4.2 km from up to bottom, and the velocities are 1.5, 2, 3 and 4.5 km/s. Three circular geometry are applied with 12.5 m equidistant receivers. All circles are centered at position (0, 13.5, 13.5) km and they have 880, 1257 and 1634 receivers for 7, 10 and 13 km of circle radius respectively. The analytical formulation gives the traveltimes per layer. In order to compare analytical and numerical traveltimes, it is necessary to register only the smaller times using all interfaces as shown in Figure 3d, where the purple line is the target of analytical times. Raypaths are shown in Figure 3c and they are calculated from the gradient of the transit time volume, for isotropic media, is perpendicular to the isochrones (Vidale, 1988). We apply the descent gradient method to find the raypath from the receiver to the source with a fixed ray step of 25 % of the minimal grid length.

In the third scheme, we study how numerical first arrivals can be correlated to waveform modeling for acoustic media performing on the SEG/EAGE Overthrust model (Lecomte et al., 1994). A smoothed version of this model is used in Noble et al. (2014) to verify accuracy of a new eikonal solver. In our study we use a version of the model without smoothing to verify wavefront similarities between acoustic wave equation and numerical first arrivals. The model dimension is (4.66, 20, 20) km and the sample spacing is 12.5 m to use frequencies high enough to perform numerical simulation with a manageable model, presenting (373, 1601, 1601) samples and almost 4 GB of storage. Figure 4 shows the third scheme configuration of the circular acquisition geometry, a central

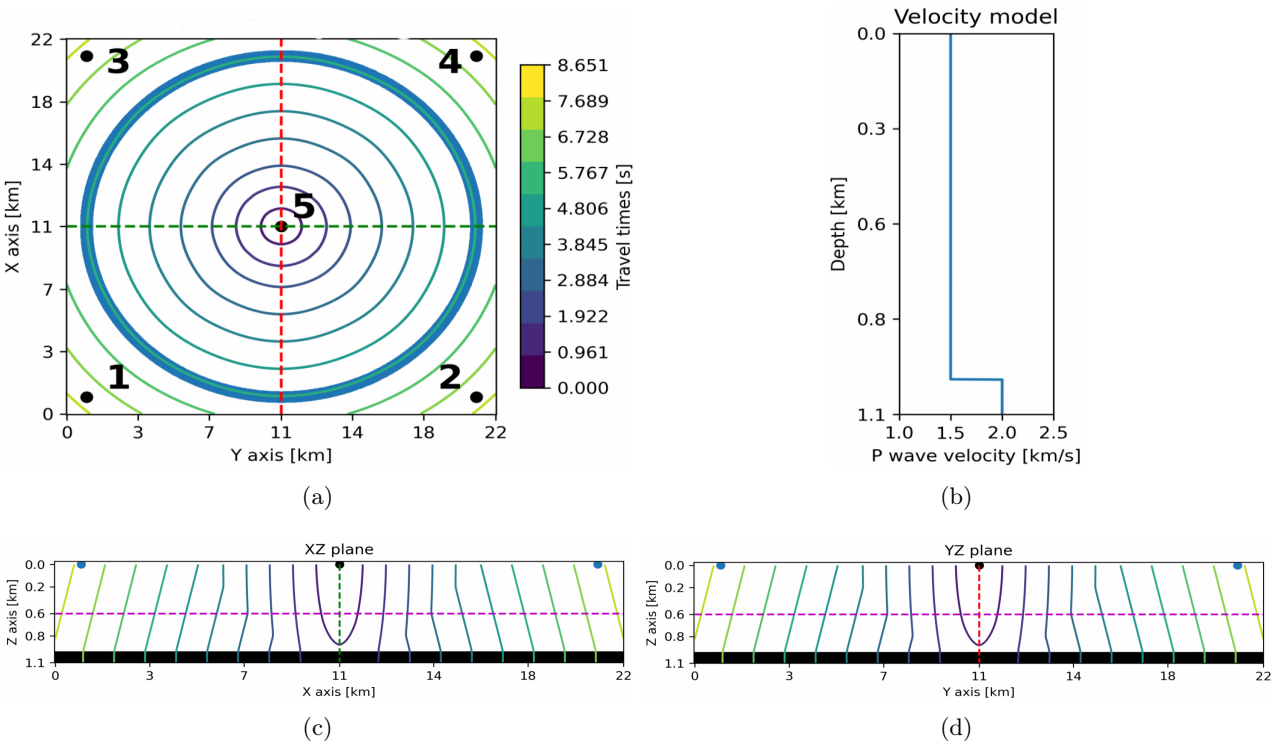

Figure 2: First scheme. (a) acquisition geometry with shot and receiver positions. The contours are traveltimes and the dotted lines indicate plane slices; (b) 1D velocity model illustrating depth interface; (c) and (d) traveltime contours and the projection of the central shot and receivers at XZ and YZ plane slices.

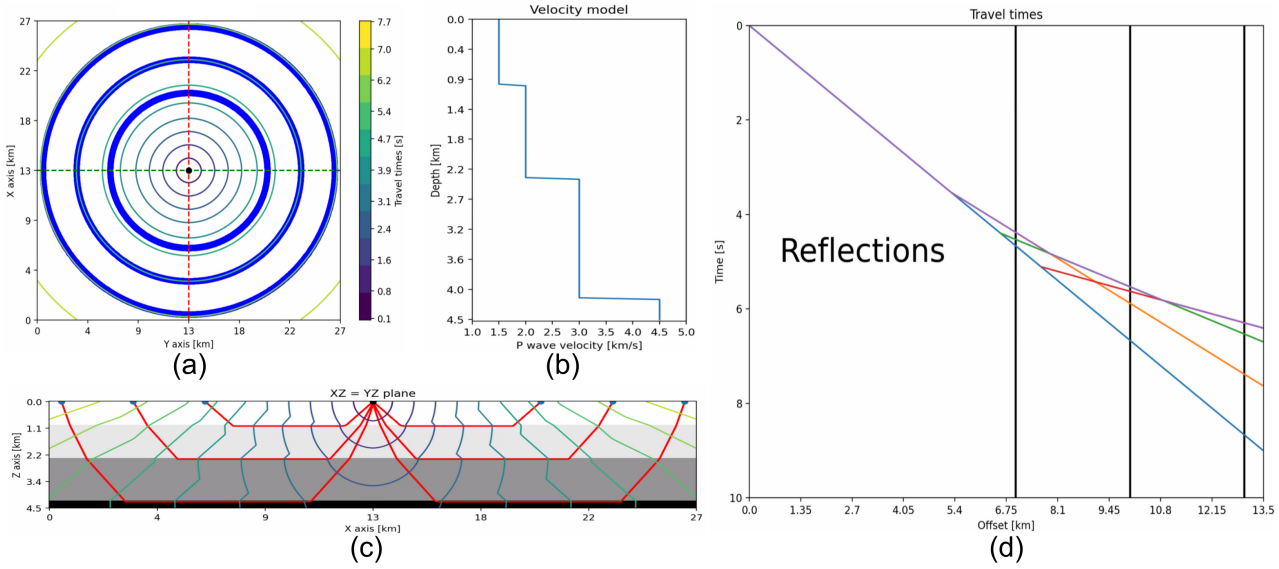

Figure 3: Second scheme. (a) all acquisition geometry with receiver circle radii of 7, 10 and 13 km. Traveltimes are delimited by a contour map; (b) 1D velocity model to show velocity contrasts at each depth; (c) 2D model slice to show raypaths from source to projected receivers; (d) Circle offset justification. For each circle, a different wavefront is registered. The smaller time is selected to build first arrival traveltimes.

log velocity and the vertical slices of the XZ and YZ plane. The velocities on the model varies from 2.5 to 6 km/s. The acquisition geometry is composed of 4 shots and 1194 receivers. The shots are positioned at 1 - (0, 0.5, 0.5); 2 - (0, 19.5, 0.5); 3 - (0, 0.5, 19.5); and 4 - (0, 19.5, 19.5) km; the receivers have a circular configuration and are spaced 50 m away from each other. The circle is centered at (0, 10, 10) km and the radius is 9.5 km. The nearest offset is 3935 m and the largest offset is 22935 m for the position of all shots.

The wave equation for isotropic acoustic media is given by:

$$\nabla^2 P - \frac{1}{v^2}\frac{\partial^2 P}{\partial t^2} = f(t), \tag{3}$$

where $P = P(z, x, y)$ is the pressure in Pascal (Pa); $v = v(z, x, y)$ is the velocity model volume; and $f(t)$ is a source applied at the (z_0, x_0, y_0) position at the time instant t. The reference source is a zero phase Ricker wavelet with 50 Hz of maximum frequency and 1 Pa of maximum amplitude. The finite difference method is applied, and we employ operators of eighth order in space and second order in time. Boundary conditions were solved using a classical absorbing condition (Cerjan et al., 1985) with 50 points and an attenuation coefficient of 0.0045 following Bording (2004) who shows the optimal way to set parameters in a sponge boundary condition. We record the waveform outside the grid using the Hicks (2002) interpolation. The total modeling time is 6 seconds and the discretization parameter is 0.8 ms to avoid finite difference numerical dispersion and maintain stability conditions.

All the results will respect the same color scheme for each eikonal solver, which is blue for Podvin and Lecomte (1991); yellow, for Jeong and Whitaker (2008); and green, for Noble et al. (2014). The line styles for each model discretization parameter are solid, dashed and dash-dotted for 25 m, 50 m and 100 m, respectively.

RESULTS AND DISCUSSION

Each scheme is discussed individually to explain its particularities. Figure 5 shows the results about the symmetry and reciprocity analysis in order to measure azimutal errors and numerical time errors. Figure 6 illustrates how traveltime errors behave when the wavefront propagates in high contrasted velocity interfaces. Scheme 3 presents the acoustic waveform propagation comparing it to numerical eikonal solutions in order to verify correlations between them.

First scheme

All the base results of the first scheme are illustrated in Figure 5, where the shot gathers for each shot position are shown in a global view (Figs. 5a, 5b, 5c and 5d) for symmetry studies and in a refined view (Figs. 5e and 5f) for accuracy and reciprocity studies.

The symmetry analysis about symmetric shots following the acquisition geometry in Figure 2 is presented in Figure 6. The vertical axis is the time error in milliseconds and the horizontal axis is the receiver indexes of a circular configuration. The symmetry study was done using the results of Figure 5a subtracted by the traveltimes in Figure 5b in their reverted indexation. This operation is shown in Figures 6a, 6c and 6e for a sample spacing of 100, 50 and 25 m, respectively. The same analysis was done for the other pair of symmetrical shots illustrated in its raw form in Figures 5c and 5d, which the results are shown in Figures 6b, 6d and 6f. The eikonal solvers respected the symmetry employed by the acquisition geometry, just the Podvin and Lecomte (1991) formulation 25 m sample spacing case that appeared some noise in a scale of 1 millisecond. It shows that the traveltimes are being computed equally in the entire circular geometry independent of the geometry direction. That is a great information to use for eikonal equation in target-oriented reservoir monitoring studies with circular geometry.

The regional accuracy study is done by computing the analytical solution subtracted by the numerical formulations for each discretization parameter shown in Figures 5a, 5b, 5c, and 5d. To optimize the figure, the symmetrical shots will be plotted at the same image where, for shots 1 and 2, the line style is solid and, for shots 3 and 4, the line style is dashed with opacity. Figure 7 shows the accuracy of traveltimes for the external shots 1, 2, 3 and 4. This analysis is possible by subtracting the analytical solution by the numerical results for each eikonal solver using a specific model sample spacing. Figure 7 presents the results with the same scale to show that traveltime errors decrease with discretization parameter refinement. It happens just because finite difference operators can generate better results with thin grid spacing. Note that the formulation with larger difference between analytic errors is the Fast Iterative Method and the formulation with the smaller errors is the accurate Fast Sweeping Method. The four external shot run times for each numerical method are registered in Table 1. According to Table 1 results, the fastest algorithm is the Fast Iterative Method. The classical formulation appears not so computationally efficient with a sample spacing of 100 m, but when the discretization parameter decreases it becomes faster than the Fast Sweeping Method. It is the implication of the hardware used to compute each method; when GPU is activated, larger parallel processes work better than larger serial processes. The storage model counts total grid points divided by 1 Mega Byte. For example, a 25 m model has $45 \times 881 \times 881 \times 4$ / 1024 / $1024 \approx 133$ MB.

The central shot of the first scheme with the accuracy and the reciprocity study is shown separately. Figure 8 shows only the accuracy results; Figure 9, the reciprocity ones. The expected behavior of the circular geometry survey with a central shot result is

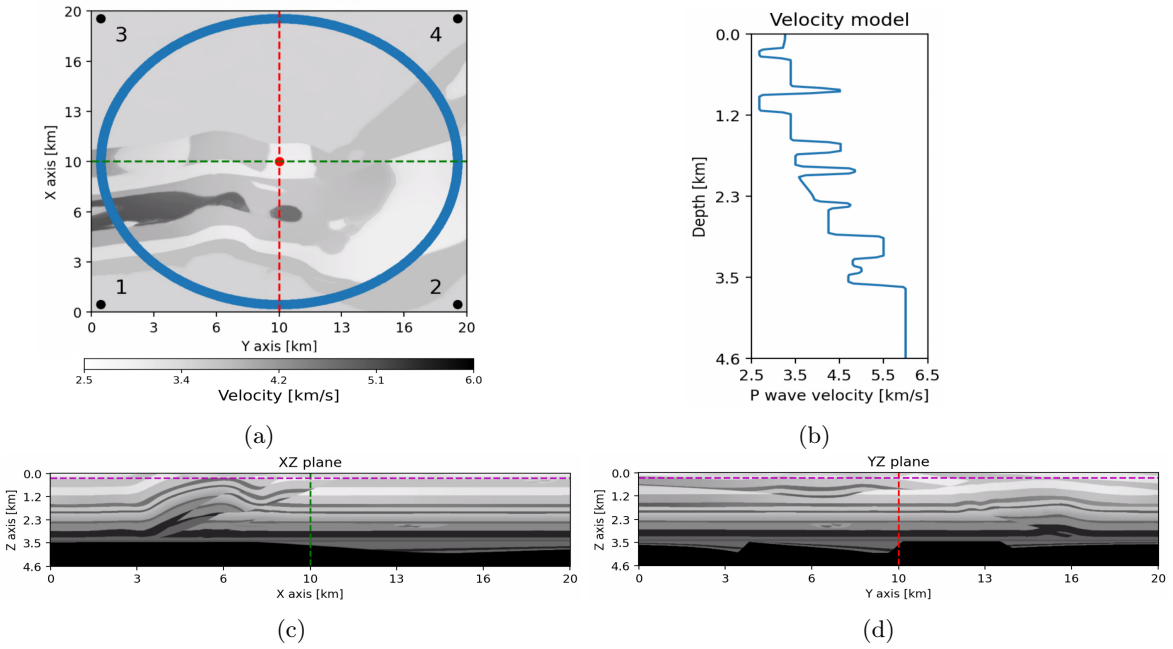

Figure 4: Third scheme: SEG/EAGE Overthrust benchmark model. (a) acquisition geometry with shot and receiver positions. The color bar represents all velocities in the model; (b) 1D velocity model log projected at the center of the model; (c) and (d) are the model XZ and YZ projections; the dotted lines indicate each projection.

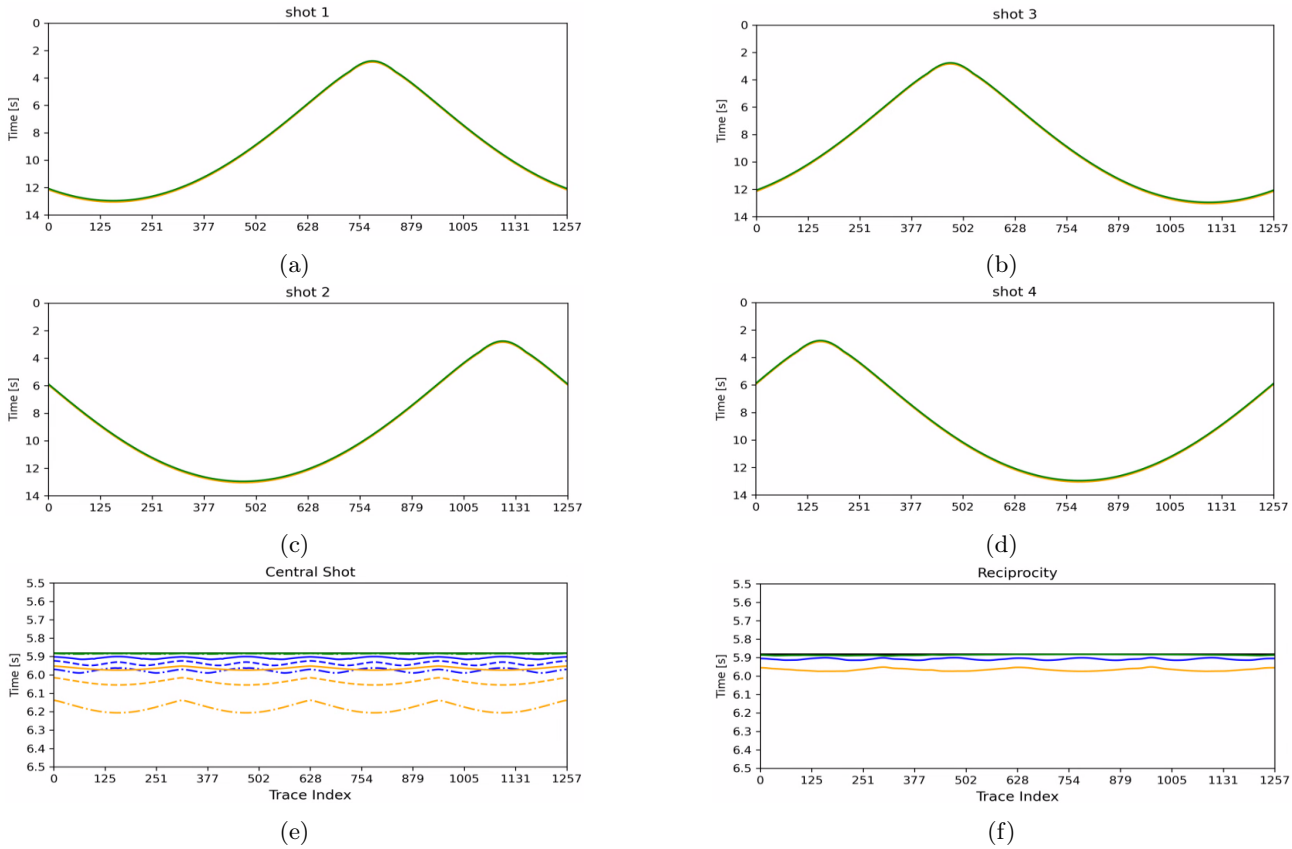

Figure 5: First scheme. Shot gathers for position 1 (a), 3 (b), 2 (c) and 4 (d) to build the symmetry studies. Shot gathers for the central position (e) and (f) to build the reciprocity and detailed accuracy studies. The colors indicate the methods and the line style indicates the model sample spacing. For colors we have blue for Podvin and Lecomte (1991); yellow, for Jeong and Whitaker (2008); and green, for Noble et al. (2014). For line styles, we have solid for 25 m; dashed, for 50 m; and dash-dotted, for 100 m. The reciprocity study was done using only the model with spatial discretization parameter of 25 m.

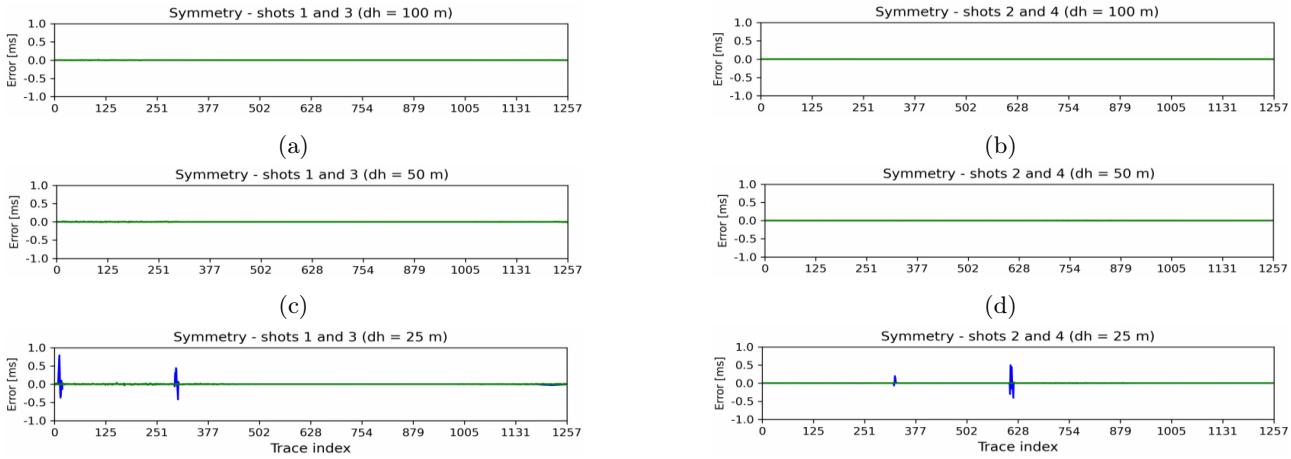

Figure 6: Symmetry results for the first scheme. (a), (c) and (e) are the symmetrical shots analyses for positions 1 and 3 with a discretization parameter of 100 m, 50 m and 25 m, respectively. (b), (d) and (f) are the symmetrical shot analyses for positions 2 and 4 with a discretization parameter of 100 m, 50 m and 25 m, respectively. The color convention of eikonal solvers is applied, but the resulted lines are overlapped. (e) and (f) present some noise artifacts but smaller than in the common seismic exploration resolution.

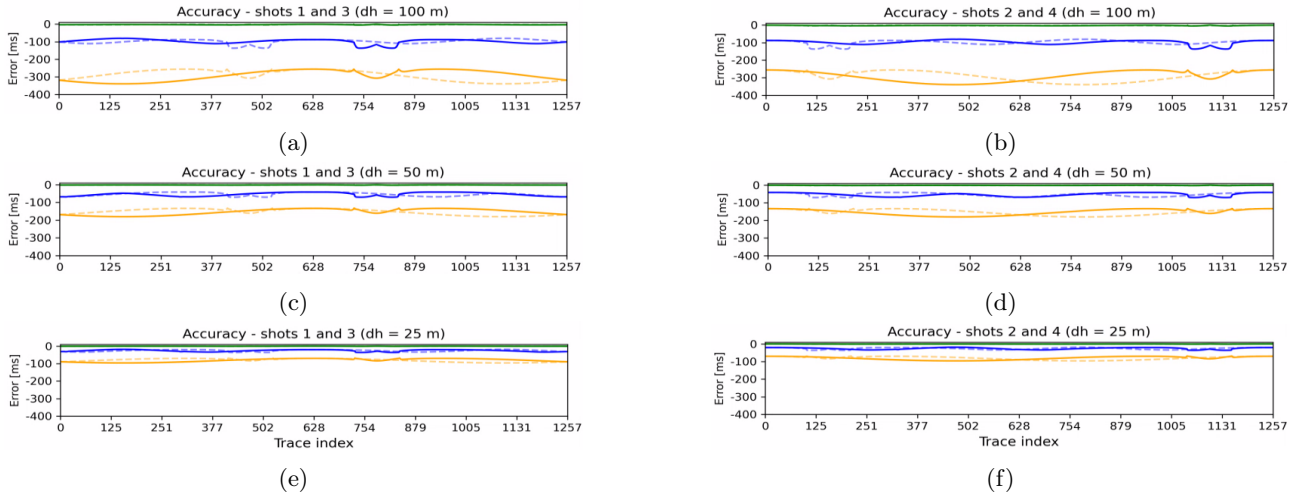

Figure 7: Accuracy results for external shots of the first scheme. (a), (c) and (e) are the accuracy of shots 1 and 3, respecting the color and line style convention: blue for Podvin and Lecomte (1991), yellow for Jeong and Whitaker (2008) and green for Noble et al. (2014). The solid lines represent the errors of shots 1 and 2. On the other hand, the dashed lines represent shots 3 and 4 errors. The scale of errors is the same to validate the error decreasing with grid refinement.

Table 1: Execution time for external shots in the first approach and the storage of each model.

	100 m	50 m	25 m
Podvin and Lecomte (1991)	4.469 s	5.557 s	60.269 s
Jeong and Whitaker (2008)	0.523 s	3.761 s	53.408 s
Noble et al. (2014)	2.485 s	12.113 s	92.937 s
Model storage	2.2 MB	17 MB	133 MB

a constant traveltime as the analytical solution computes. The analytical equation shows that for the central shot the traveltime response is a constant time for all receivers. Looking carefully at Figures 8a, 8b and 8c, the maximum difference error registered occurs at −120, −350 and −5 ms, respectively. Because of that, the most accurate method is the Noble et al. (2014) formulation for this case due to the magnitude of difference between analytical and numerical solutions.

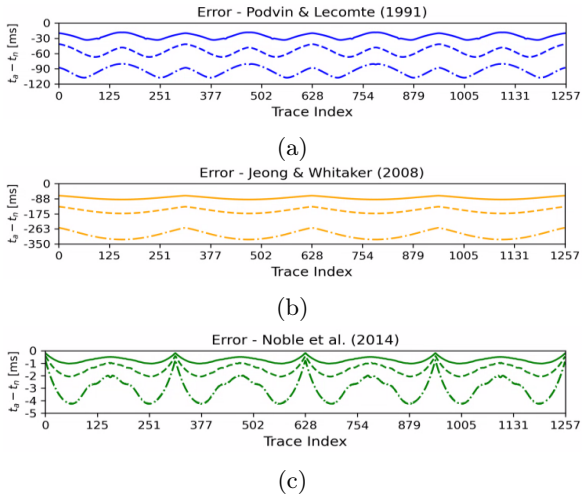

Figure 8: Central shot error comparison for the first scheme. (a) Podvin and Lecomte (1991), (b) Jeong and Whitaker (2008); and (c) Noble et al. (2014) formulations. The line styles represent the model sample spacing, where solid lines are for 25 m; dashed, for 50 m; and dash-dotted; for 100 m spacing.

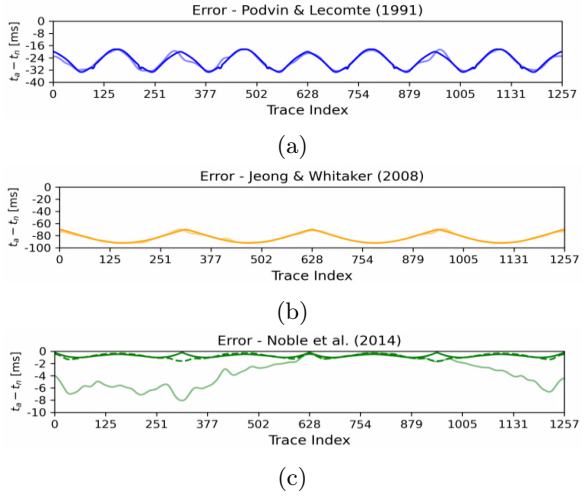

Figure 9: Reciprocal time accuracy study for the first scheme. The solid lines represent the shot to receiver records and the opaque ones, the receiver to shot records. (a) Podvin and Lecomte (1991); (b) Jeong and Whitaker (2008); and (c) Noble et al. (2014) formulations. The dashed line in part (c) represents the adjusted traveltimes caused by a wrong initialization in the Noble et al. (2014) algorithm.

Figure 9 shows the reciprocity traveltime error behavior comparison for the sample spacing of 25 m. The results in Figures 9a and 9b fit well between forward and reciprocity traveltimes and in Figure 9 the difference had initially huge errors. These errors are caused because the Fast Sweeping Method was not initialized perfectly at all possible directions. When we start the eikonal solution, an initialization computes the analytical traveltime to fill all points surrounding the source with the exact solution. After that, the traveltimes respect the reciprocity principle very well (Fiure 9c - dashed line). The sinuous behavior in all traveltimes happens because the Cartesian coordinate has an intrinsic azimutal imprecision (Alkhalifah and Fomel, 2001; White et al., 2020). The run time of the central shot for all numerical methods and the reciprocity run time for 1257 shots are shown in Table 2. The estimated reciprocity run time is computed based on the run time of the sample spacing of 25 m.

Table 2: Execution run time for the central shot in the first approach and its estimated reciprocity and run time.

	Podvin (1991)	Jeong (2008)	Noble (2014)
100m	1.171 s	0.379 s	0.808 s
50m	2.052 s	1.132 s	3.747
25m	10.416 s	8.211 s	22.794 s
Estimated reciprocity	3 h 38 min 12 s	2 h 52 min 5 s	7 h 57 min 32 s
Reciprocity run	3 h 22 min 38 s	2 h 43 min 25 s	7 h 12 min 34 s

Second scheme

The results of the second scheme appear in Figure 10 from the acquisition geometry shown in Figure 3. It is used three geometry circles with radii of 7, 10 and 13 km shown in Figures 10a, 10b and 10c respectively. Each gather reveals the results of the traveltime difference between the analytical equations at the same error scale.

Noble et al. (2014) formulation errors are close to zero and the other ones, Podvin and Lecomte (1991) and Jeong and Whitaker (2008) formulations, have average errors of −25 ms and −80 ms, respectively. However, in Figure 10b and 10c, when the wavefront propagates through more interfaces, while the Noble et al. (2014) formulation increases its errors, the Podvin and Lecomte (1991) and the Jeong and Whitaker

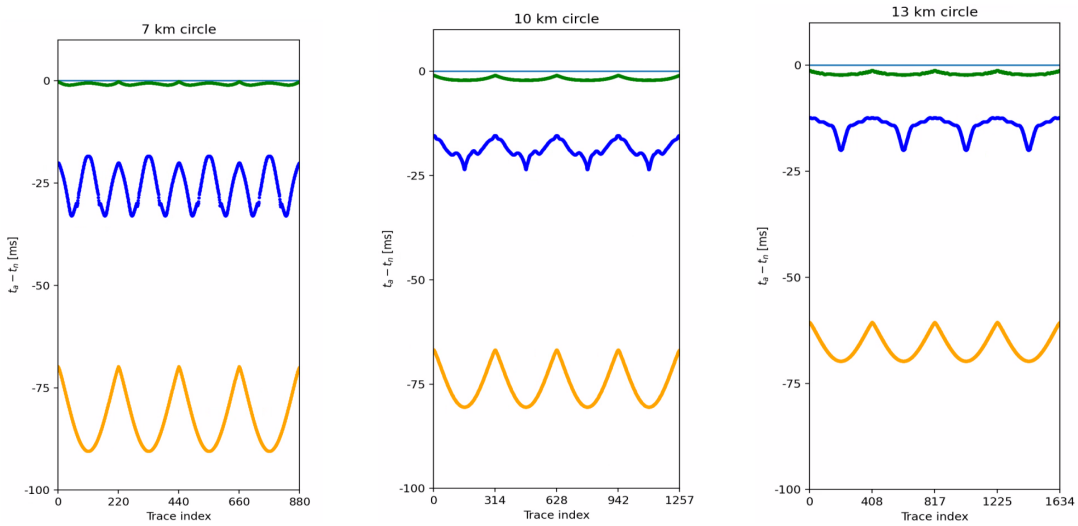

(a) (b) (c)

Figure 10: Resulting gathers for the central shot in approach 2: difference of analytical first arrival traveltimes. All numerical methods are shown using only the model sample spacing of 25 m. (a) nearest circle offset with 7 km; (b) mid circle offset with 10 km; and (c) longest offset with 13 km. The line colors indicate each method: blue for Podvin and Lecomte (1991), yellow for Jeong and Whitaker (2008) and green for Noble et al. (2014).

(2008) formulations decrease their errors. The expected behavior is to decrease the precision when the number of layers increases.

Table 3: Run time execution for a central shot using approach 2, the model with three interfaces.

Podvin and Lecomte (1991)	93.055 s
Jeong and Whitaker (2008)	62.491 s
Noble et al. (2014)	129.303 s
Model storage	807 MB

The errors observed with Noble et al. (2014) have almost the same scale in Figures 10a, 10b and 10c. For complex models, the result might be as accurate as using simple models. The hardware used to compute run time execution in Tables 1, 2, 3 and 4 are the CPU Intel Xeon E-2288G (3.7 GHz) and the GPU Nvidia Quadro 4000 (8 GB). Table 3 shows the run time execution for the three numerical methods using a model with $181 \times 1081 \times 1081$ samples. Once again, the Jeong and Whitaker (2008) formulation performs better than the other formulations.

Third scheme

Figure 11 shows the shot 1 in the configuration presented in Figure 4. Four windows (Figure 11a) are positioned strategically on the seismogram to verify the correlations between the first arrivals computed by the wave propagation and the traveltimes calculated via eikonal solvers. Figures 11b, 11c, 11d and 11e show the windows with their respective signals, red and green, to point out bad and good correlations with numeric seismic waves. Figures 12, 13 and **??** follow the same pattern to verify all directions of propagation in the SEG/EAGE Overthrust model. The target first arrivals registered in the seismograms are the first black amplitude because of the zero phase wavelet applied.

A visual correlation is done and we noticed that in the nearest offsets a good correlation between the seismic and the numerical first arrivals appears in Figures 12e, 13c and 14b. Only in Figure 11d the nearest offsets have anomalous traveltimes showing smaller results than the finite difference solution for a complete wave equation. The bad correlations may be caused by the thin layers in the model. The eikonal equation may represent that high velocity thin layers better than the complete finite difference wave equation solution using a maximum frequency of 50 Hz. Long offsets have good correlation as show in Figure 12c, but not in Figures 11b, 13e and 14d. The most part of the correlation, pointed with green arrows, are good, although some red arrows show bad correlations in near and far offsets. In general, considering low frequency wave propagation, high offsets and a model with high velocity thin layers, the correlation between wave equation and eikonal solvers is acceptable for seismic applications.

To verify performance, the comparison between numerical method run times, inclusive the wave equation solver algorithm and the model size in MB, is shown in Table 4. Computationally, it is cheaper solving eikonal equations than acoustic wave ones. Due to the computational effort required to run the methods, the hardware used to execute the program are now the CPU Intel Xeon Gold 6248R (3.0 GHz) and

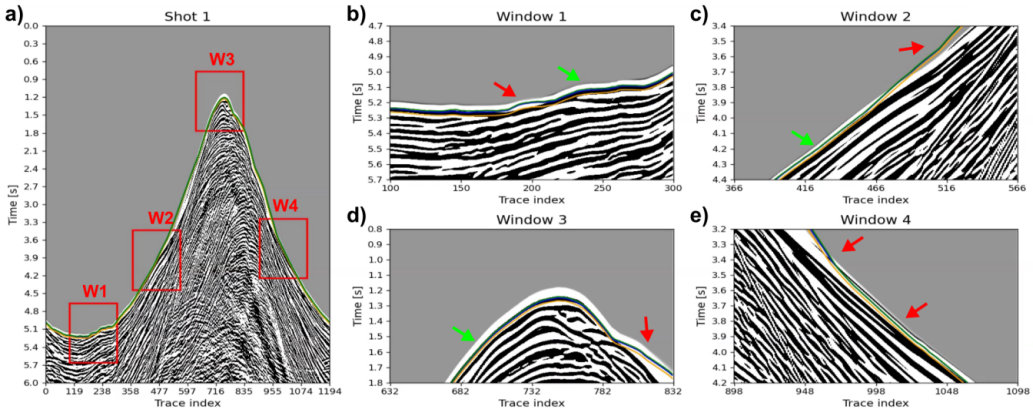

Figure 11: Shot 1 in approach 3. (a) 6 seconds of seismic data behavior. All zoom windows are shown at a specific position; (b), (c), (d) and (e) are the zoom window plots to show good (green arrows) and bad (red arrows) correlations between seismic data and first arrival traveltimes. The methods are plotted in blue (Podvin and Lecomte, 1991), yellow (Jeong and Whitaker, 2008) and green (Noble et al., 2014) lines.

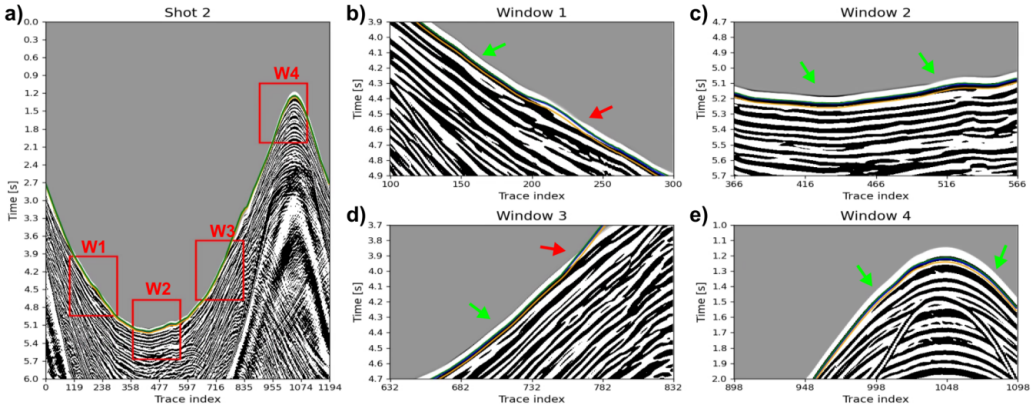

Figure 12: Shot 2 in approach 3. (a) 6 seconds of seismic data behavior. All zoom windows are shown at a specific position; (b), (c), (d) and (e) are the zoom window plots to show good (green arrows) and bad (red arrows) correlations between seismic data and first arrival traveltimes. The methods are plotted in blue (Podvin and Lecomte, 1991), yellow (Jeong and Whitaker, 2008) and green (Noble et al., 2014) lines.

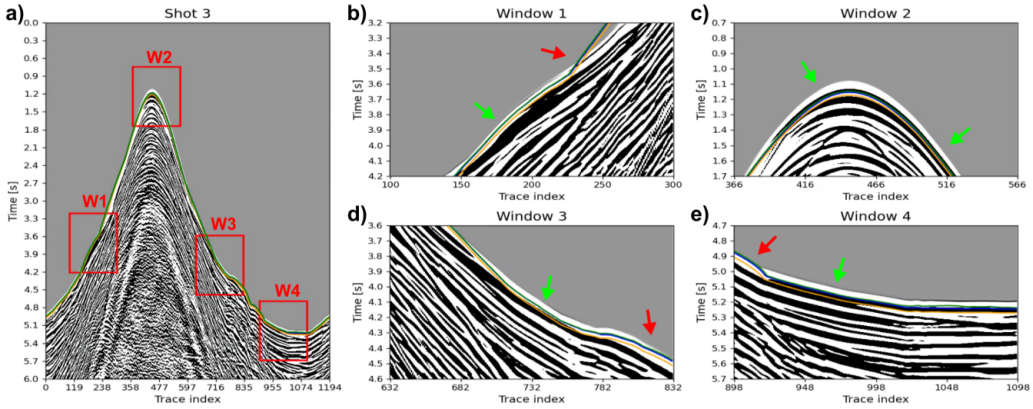

Figure 13: Shot 3 in approach 3. (a) 6 seconds of seismic data behavior. All zoom windows are shown at a specific position. (b), (c), (d) and (e) are the zoom window plots to show good (green arrows) and bad (red arrows) correlations between seismic data and first arrival traveltimes. The methods are plotted in blue (Podvin and Lecomte, 1991), yellow (Jeong and Whitaker, 2008) and green (Noble et al., 2014) lines.

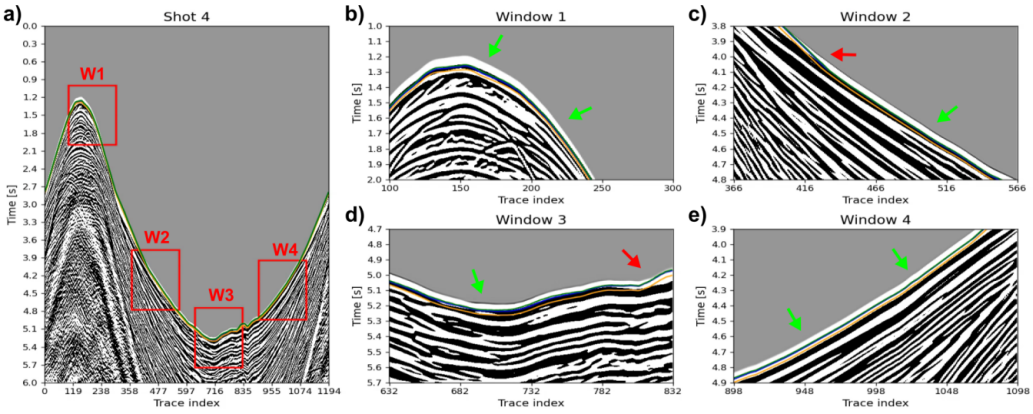

Figure 14: Shot 4 in approach 3. (a) 6 seconds of seismic data behavior. All zoom windows are shown at a specific position; (b), (c), (d) and (e) are the zoom window plots to show good (green arrows) and bad (red arrows) correlations between seismic data and first arrival traveltimes. The methods are plotted in blue (Podvin and Lecomte, 1991), yellow (Jeong and Whitaker, 2008) and green (Noble et al., 2014) lines.

the GPU Quadro RTX 6000 (22 GB).

Table 4: Four shot run time comparison for approach 3 including wave equation solver and model size.

Podvin and Lecomte (1991)	39 min 40 s
Jeong and Whitaker (2008)	34 min 50 s
Noble et al. (2014)	40 min 28 s
Wave equation	3 h 5 min 27 s
Model storage	3647 MB

Figure 15 shows the difference between Noble et al. (2014) formulation and the other methods. For each shot, the traveltimes of the modified Fast Sweeping Method is subtracted by the classic and the Fast Iterative Method. A mean error per shot is done collecting the traveltimes per trace and dividing by the total number of traces. The average difference between the Noble et al. (2014) and the Podvin and Lecomte (1991) formulations is smaller than the difference from the Noble et al. (2014) and the Jeong and Whitaker (2008) ones. The traveltime differences are always negative, so the methods present the same aspects shown in approaches 1 and 2. Podvin and Lecomte (1991) present better results for high contrast model with a mean difference of -6 ms. The Fast Iterative Method traveltimes present a higher mean error and it can cause a wrong seismic analysis when used as a kernel of some methodology.

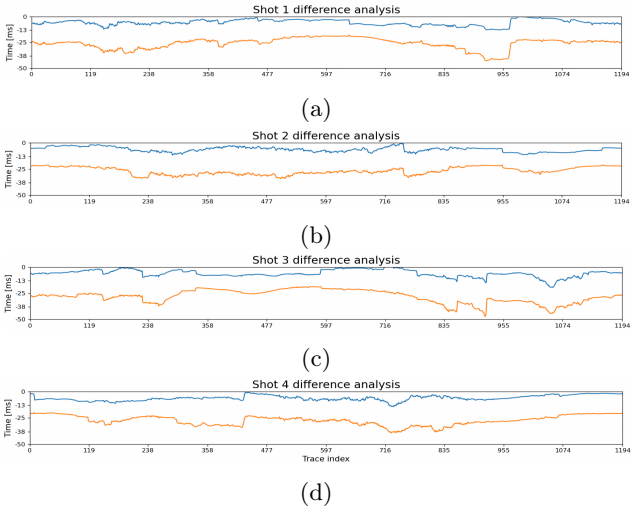

Figure 15: Comparison of differences between the Noble et al. (2014) and the Podvin and Lecomte (1991) formulations and between the Noble et al. (2014) and the Jeong and Whitaker (2008) to verify the traveltime discrepancy assuming Noble et al. (2014) as the most accurate solver. The difference in milliseconds is negative. In other words, the classic and the Fast Iterative methods present a traveltime higher than the Fast Sweeping Method.

CONCLUSION

From the results among comparisons of Podvin and Lecomte (1991), Jeong and Whitaker (2008), and Noble et al. (2014) formulations to solve the eikonal equation, the most accurate method is presented as the modified Fast Sweeping Method. Three approaches are applied and, in large scale situations, as shown in approach 3, the most accurate method does not differ too much in performance from the others. Then this Fast Sweeping Method can be applied on huge simulations. The classic method shows great differences between the reference traveltime in

approaches 1 and 2. However, for approach 3, with a complex model, Podvin and Lecomte (1991) formulation does not exhibit significant differences from the most accurate solver. Then, the classic formulation still appears as a great eikonal solver in strongly heterogeneous media. The Fast Iterative Method demonstrates the highest performance and a smaller precision in all studied cases. So, this method may be used when the traveltimes precision is not necessary, such as a pathfinding problem. A future work suggestion is to verify the improved Fast Iterative Method solution to check accuracy compared with the GPU implementation of the accurate Fast Sweeping Method. Accuracy and performance on seismic imaging experiments, such as tomography or depth migration, could be taken into account to verify the best method applicability.

REFERENCES

Ahmed, S., S. Bak, J. McLaughlin, and D. Renzi, 2011, A third order accurate fast marching method for the eikonal equation in two dimensions: SIAM Journal on Scientific Computing, **33**, 2402–2420, doi: https://doi.org/10.1137/10080258X.

Alkhalifah, T., and S. Fomel, 2001, Implementing the fast marching eikonal solver: spherical versus cartesian coordinates: Geophysical Prospecting, **49**, 165–178, doi: https://doi.org/10.1046/j.1365-2478.2001.00245.x.

Bak, S., J. McLaughlin, and D. Renzi, 2010, Some improvements for the fast sweeping method: SIAM Journal on Scientific Computing, **32**, 2853–2874, doi: https://doi.org/10.1137/090749645.

Balkaya, Ç., Z. Akçığ, and G. Göktürkler, 2010, A comparison of two travel-time tomography schemes for crosshole radar data: Eikonal-equation-based inversion versus ray-based inversion: Journal of Environmental & Engineering Geophysics, **15**, 203–218, doi: https://doi.org/10.2113/JEEG15.4.203.

Bording, R. P., 2004, Finite difference modeling - nearly optimal sponge boundary conditions: Presented at the 2004 SEG Annual Meeting, SEG Technical Program Expanded Abstracts. Denver, Colorado. doi: https://doi.org/10.1190/1.1845189.

Bulhões, F. C., M. A. C. Santos, L. A. Santos, and V. T. X. de Almeida, 2021, Regularization effects on 2D seismic refraction tomography: case study on shallow marine environment: Presented at the 17th International Congress of the Brazilian Geophysical Society, SBGf. Rio de Janeiro, Brazil.

Cai, W., P. Zhu, and G. Li, 2023, Improved fast iterative method for higher calculation accuracy of traveltimes: Computers & Geosciences, **174**, 105331, doi: https://doi.org/10.1016/j.cageo.2023.105331.

Capozzoli, A., C. Curcio, A. Liseno, and S. Savarese, 2013, A comparison of fast marching, fast sweeping and fast iterative methods for the solution of the eikonal equation: 2013 21st Telecommunications Forum Telfor (TELFOR), IEEE, Belgrade, Serbia, 685–688. doi: https://doi.org/10.1109/TELFOR.2013.6716321.

Cerjan, C., D. Kosloff, R. Kosloff, and M. Reshef, 1985, A nonreflecting boundary condition for discrete acoustic and elastic wave equations: Geophysics, **50**, 705–708, doi: https://doi.org/10.1190/1.1441945.

Cervenỳ, V., 2001, Seismic ray theory: Cambridge University Press, Cambridge, doi: https://doi.org/10.1017/CBO9780511529399.

Costa, F., F. Capuzzo, A. de Souza Jr, R. Moreira, J. Lopez, and M. Cetale, 2020, Understanding refracted wave paths for Brazilian pre-salt target-oriented imaging, *in* SEG Technical Program Expanded Abstracts 2020. Virtual event: Society of Exploration Geophysicists, 2375–2380. doi: https://doi.org/10.1190/segam2020-3426868.1.

Da Silva, S., A. Karsou, R. Moreira, J. Lopez, and M. Cetale, 2022, Klein-Gordon equation and variable density effects on acoustic wave propagation in Brazilian pre-salt fields: 83rd EAGE Annual Conference & Exhibition, European Association of Geoscientists & Engineers, Madrid, 1–5. doi: https://doi.org/10.3997/2214-4609.202210385.

Dang, F., and N. Emad, 2014, Fast iterative method in solving eikonal equations: a multi-level parallel approach: Procedia Computer Science, **29**, 1859–1869, doi: https://doi.org/10.1016/j.procs.2014.05.170.

De Matteis, R., A. Romeo, G. Pasquale, G. Iannaccone, and A. Zollo, 2010, 3D tomographic imaging of the southern apennines (Italy): A statistical approach to estimate the model uncertainty and resolution: Studia Geophysica et Geodaetica, **54**, 367–387, doi: https://doi.org/10.1007/s11200-010-0022-x.

Detrixhe, M., F. Gibou, and C. Min, 2013, A parallel fast sweeping method for the eikonal equation: Journal of Computational Physics, **237**, 46–55, doi: https://doi.org/10.1016/j.jcp.2012.11.042.

Farber, R., 2016, Parallel programming with openacc: Newnes, doi: https://doi.org/10.1016/B978-0-12-410397-9.00001-9.

Farra, V., 1993, Ray tracing in complex media: Journal of Applied Geophysics, **30**, 55–73, doi: https://doi.org/10.1016/0926-9851(93)90018-T.

Herrmann, M., 2003, A domain decomposition parallelization of the fast marching method: Technical Report: Presented at the Defense Technical Information Center.

Hicks, G. J., 2002, Arbitrary source and receiver positioning in finite-difference schemes using Kaiser windowed sinc functions: Geophysics, **67**, 156–165, doi: https://doi.org/10.1190/1.1451454.

Hole, J., and B. Zelt, 1995, 3-D finite-difference reflection traveltimes: Geophysical Journal International, **121**, 427–434, doi: https://doi.org/10.1111/j.1365-

246X.1995.tb05723.x.

Hong, S., and W.-K. Jeong, 2016, A multi-gpu fast iterative method for eikonal equations using on-the-fly adaptive domain decomposition: Procedia Computer Science, **80**, 190–200, doi: https://doi.org/10.1016/j.procs.2016.05.309.

Huang, G., and S. Luo, 2020, Hybrid fast sweeping methods for anisotropic eikonal equation in two-dimensional tilted transversely isotropic media: Journal of Scientific Computing, **84**, 1–30, doi: https://doi.org/10.1007/s10915-020-01280-3.

Huang, Y., 2021, Improved fast iterative algorithm for eikonal equation for GPU computing (version 3): arXiv, doi: https://doi.org/10.48550/ARXIV.2106.15869.

Jeong, W.-K., and R. T. Whitaker, 2008, A fast iterative method for eikonal equations: SIAM Journal on Scientific Computing, **30**, 2512–2534, doi: https://doi.org/10.1137/060670298.

Kearey, P., M. Brooks, and I. Hill, 2002, An introduction to geophysical exploration, **4**: John Wiley & Sons.

Koketsu, K., 2000, Finite difference traveltime calculation for head waves travelling along an irregular interface: Geophysical Journal International, **143**, 729–734, doi: https://doi.org/10.1046/j.1365-246X.2000.00269.x.

Lecomte, J., E. Campbell, and J. Letouzey, 1994, Building the *SEG/EAGE* overthrust velocity macro model: EAGE/SEG Summer Workshop-Construction of 3-D Macro Velocity-Depth Models, European Association of Geoscientists & Engineers, cp–96. doi: https://doi.org/10.3997/2214-4609.201407587.

Linde, N., A. Tryggvason, J. E. Peterson, and S. S. Hubbard, 2008, Joint inversion of crosshole radar and seismic traveltimes acquired at the south oyster bacterial transport site: Geophysics, **73**, G29–G37, doi: https://doi.org/10.1190/1.2937467.

Lopez, J., F. Neto, M. Cabrera, S. Cooke, S. Grandi, and D. Roehl, 2020, Refraction seismic for pre-salt reservoir characterization and monitoring: Presented at the SEG International Exposition and Annual Meeting. Virtual event, SEG Technical Program Expanded Abstracts. doi: https://doi.org/10.1190/segam2020-3426667.1.

Luo, S., and J. Qian, 2012, Fast sweeping methods for factored anisotropic eikonal equations: multiplicative and additive factors: Journal of Scientific Computing, **52**, 360–382, doi: https://doi.org/10.1007/s10915-011-9550-y.

Noble, M., A. Gesret, and N. Belayouni, 2014, Accurate 3-D finite difference computation of traveltimes in strongly heterogeneous media: Geophysical Journal International, **199**, 1572–1585, doi: https://doi.org/10.1093/gji/ggu358.

Podvin, P., and I. Lecomte, 1991, Finite difference computation of traveltimes in very contrasted velocity models: a massively parallel approach and its associated tools: Geophysical Journal International, **105**, 271–284, doi: https://doi.org/10.1111/j.1365-246X.1991.tb03461.x.

Qin, F., Y. Luo, K. B. Olsen, W. Cai, and G. T. Schuster, 1992, Finite-difference solution of the eikonal equation along expanding wavefronts: Geophysics, **57**, 478–487, doi: https://doi.org/10.1190/1.1443263.

Rawlinson, N., and M. Sambridge, 2004, Wave front evolution in strongly heterogeneous layered media using the fast marching method: Geophysical Journal International, **156**, 631–647, doi: https://doi.org/10.1111/j.1365-246X.2004.02153.x.

Rawlinson, N., and M. Sambridge, 2005, The fast marching method: an effective tool for tomographic imaging and tracking multiple phases in complex layered media: Exploration Geophysics, **36**, 341–350, doi: https://doi.org/10.1071/EG05341.

Robinson, E. A., and D. Clark, 2017, Basic geophysics: Society of Exploration Geophysicists. Geophysical Monograph Series, 22, 376 pp, doi: https://doi.org/10.1190/1.9781560803461.

Sethian, J. A., 1999, Fast marching methods: SIAM review, **41**, 199–235, doi: https://doi.org/10.1137/S0036144598347059.

Shen, Y., and J. Zhang, 2020, Refraction wavefield migration: Geophysics, **85**, Q27–Q37, doi: https://doi.org/10.1190/geo2020-0141.1.

Sheriff, R. E., and L. P. Geldart, 1995, Exploration seismology: Cambridge University Press, doi: https://doi.org/10.1017/CBO9781139168359.

Tryggvason, A., and B. Bergman, 2006, A traveltime reciprocity discrepancy in the Podvin & Lecomte *time3d* finite difference algorithm: Geophysical Journal International, **165**, 432–435, doi: https://doi.org/10.1111/j.1365-246X.2006.02925.x.

Van Trier, J., and W. W. Symes, 1991, Upwind finite-difference calculation of traveltimes: Geophysics, **56**, 812–821, doi: https://doi.org/10.1190/1.1443099.

Vidale, J., 1988, Finite-difference calculation of travel times: Bulletin of the Seismological Society of America, **78**, 2062–2076, doi: 10.1785/BSSA0780062062.

Waheed, U. B., and T. Alkhalifah, 2017, A fast sweeping algorithm for accurate solution of the tilted transversely isotropic eikonal equation using factorization: Geophysics, **82**, WB1–WB8, doi: https://doi.org/10.1190/geo2016-0712.1.

Waheed, U. B., C. E. Yarman, and G. Flagg, 2015, An iterative, fast-sweeping-based eikonal solver for 3D tilted anisotropic media: Geophysics, **80**, C49–C58, doi: https://doi.org/10.1190/geo2014-0375.1.

White, M. C., H. Fang, N. Nakata, and Y. Ben-Zion, 2020, Pykonal: a python package for solving the eikonal equation in spherical and Cartesian coordinates using the fast marching method: Seismological Research Letters, **91**, 2378–2389, doi:

https://doi.org/10.1785/0220190318.

Yang, J., and F. Stern, 2017, A highly scalable massively parallel fast marching method for the eikonal equation: Journal of Computational Physics, **332**, 333–362, doi: https://doi.org/10.1016/j.jcp.2016.12.012.

Yordkayhun, S., A. Tryggvason, B. Norden, C. Juhlin, and B. Bergman, 2009, 3D seismic traveltime tomography imaging of the shallow subsurface at the CO2SINK project site, Ketzin, Germany: Geophysics, **74**, G1–G15, doi: https://doi.org/10.1190/1.3026553.

Zhao, H., 2005, A fast sweeping method for eikonal equations: Mathematics of Computation, **74**, 603–627, doi: https://doi.org/10.1090/S0025-5718-04-01678-3.

Zhao, H., 2007, Parallel implementations of the fast sweeping method: Institute of Computational Mathematics and Scientific / Engineering Computing, 25, 4, 421–429, doi: https://www.jstor.org/stable/43693378.

Alves, P. H. B.: code development,methodology, writing - original draft,review and editing; **Santos, L. A**: writing - review and editing; **Capuzzo, F. V.**: initial code development; **Cetale, M.**: writing - review and editing.

Received on March 28, 2023 / Accepted on May 23, 2023